ISSN 1067-8212, Russian Journal of Non-Ferrous Metals, 2018, Vol. 59, No. 1, pp. 32–41. © Allerton Press, Inc., 2018.
Original Russian Text © A.V. Koltygin, V.E. Bazhenov, N.V. Letyagin, V.D. Belov, 2017, published in Izvestiya Vysshikh Uchebnykh Zavedenii, Tsvetnaya Metallurgiya, 2017, No. 6, pp. 20–30.

The Influence of Composition and Heat Treatment on the Phase Composition and Mechanical Properties of ML19 Magnesium Alloy

A. V. Koltygin*, V. E. Bazhenov, N. V. Letyagin***, and V. D. Belov******

National University of Science and Technology "MISiS", Moscow, 119049 Russia

**e-mail: misistlp@mail.ru*

***e-mail: V.E.Bagenov@gmail.com*

****e-mail: n.v.letyagin@gmail.com*

*****e-mail: vdbelov@mail.ru*

Received July 28, 2017; in final form, September 5, 2017; accepted for publication September 11, 2017

Abstract—Samples of ML19 magnesium alloy with composition, wt %, (0.1–0.6)Zn–(0.4–1.0)Zr–(1.6–2.3)Nd–(1.4–2.2)Y have been investigated. The influence of Nd, Y, Zn, and Zr on equilibrium phase-transition temperatures and phase composition using Thermo-Calc software is established. The Scheil–Gulliver solidification model is also used. We show the significant liquidus temperature increase if the zirconium content in alloy is higher than (0.8–0.9) wt %. Thus, a higher melting temperature is required (more than 800°C). This is undesirable when melting in a steel crucible. The change in equilibrium fractions of phases at different temperatures in ML19 magnesium alloy with a minimum and maximum amount of alloying elements are calculated. Microstructures of alloys with different amounts of alloying elements in as-cast and heat-treated condition has been studied using scanning electron microscopy (SEM). We investigate the concentration profile of Nd, Y, Zn, and Zr in the dendritic cell of an as-cast alloy. The amount of neodymium and zinc on dendritic cell boundaries increased. A high concentration of yttrium is observed both in the center and on the boundaries of the dendritic cell. A high zirconium concentration is mainly observed in the center of the dendritic cells. A small amount of yttrium is also present in zirconium particles. These particles act as nucleation sites for the magnesium solid solution (Mg) during solidification. The effect of aging temperature (200 and 250°C) on the hardness of the samples after quenching was studied. Aging at 200°C provides a higher hardness. The change in the hardness of quenched samples during aging at 200°C is investigated. Maximum hardness is observed in samples aged for 16–20 h. The two-stage solution heat treatment for 2 h at 400°C and 8 h at 500°C with water quenching and aging at 200°C for 16 h is performed. This heat treatment enables us to get tensile strength 306 ± 8 MPa and yield strength 161 ± 1 MPa with elongation 8.7 ± 1.6%.

Keywords: magnesium cast alloys, ML19, Mg–Zr–RE, Mg–Zr–Nd–Y–Zn, solidification, heat treatment, phase composition, Thermo-Calc

DOI: 10.3103/S1067821218010091

INTRODUCTION

Magnesium of the lightest of metals is used as the basis for construction materials; therefore, its alloys are most often used in fields where lightweight parts are important, such as aviation, instrument making, and the automobile industry [1, 2]. Special attention is paid to alloys based on the Mg–Zr–REM system (REMs are Nd, Y, Gd, Dy, etc.). They have a favorable combination of high mechanical properties at room temperature and a temperature elevated up to 250°C (up to 300°C for a short time) with a rather good corrosion resistance and manufacturability [3, 4].

Alloys containing Nd and Y are most widespread in industry [5]. Neodymium is one of most efficient strengthening element for magnesium among REMs of the cerium group [3, 6]. These materials are well-strengthened during heat treatment [7]. Strengthening occurs due to the high solubility of yttrium and neodymium in the magnesium solid solution at a temperature close to solidus, which strongly decreases when lowering the alloy temperature [3, 8–10]. Usually, industrial alloys with neodymium and yttrium (WE54 and WE43) contain approximately 5% Y, 2% Nd, and 2% of heavy rare-earth elements[1]. Some authors note that the yttrium addition into the ML10 alloy of the Mg–Zn–Zr–Nd system increases creep rupture strength at an elevated temperature due to the forma-

[1] Here and below, if another value is not noted, the content of elements in alloys is presented in wt %.

Table 1. Chemical composition of the ML19 alloy and its analogs

Alloy	Content of elements, wt %				
	Zn	Zr	Nd	Y	other
ML19	0.1–0.6	0.4–1.0	1.6–2.3	1.4–2.2	
Elektron WE54	–	≥0.4	1.5–2.0	4.75–5.5	1.0–2.0 heavy REMs (Yb, Er, Dy, Gd)
Elektron WE43B	–	≥0.4	–	3.7–4.3	2.4–4.4 ∑ REMs

tion of (MgZn)Y and $Mg_{24}Y_5$ compounds, but somewhat decreases the strength at room temperature [11]. Therefore, the main direction of using such materials is the fabrication of castings operating at elevated temperatures. Due to the presence of zirconium in alloys of the Mg–Zr–REM system, their castings have a homogeneous fine-grain structure [12, 13].

Most widespread alloys of magnesium with neodymium and yttrium, WE54 and WE43 (Table 1), have a ultimate strength in T6 condition at a room temperature of 275 MPa, yield strength of 200 MPa, and elongation of 4% [14]. The T6 heat treatment includes high-temperature solution treatment for 8 h at 525°C with quenching in water and subsequent aging for 16 h at 250°C [15]. The strengthening mechanism of alloys of magnesium with yttrium and neodymium is associated with the formation of metastable phases shaped as platelets and spheroids from the magnesium solid solution (Mg) [16, 17]. Some authors affirm that, in order to attain the maximal strengthening at room temperature, the aging temperature should be decreased from 250 to 210°C, which will lead to the formation numerous precipitations of strengthening metastable phases [18, 19].

The ML19 alloy (*GOST* (State Standard) *2856–79*) contains a smaller amount of yttrium (Table 1) than WE54 and WE43, but a small amount of zinc, which is absent in other widespread alloys with yttrium, is present. The presence of zinc positively affects the strength of the ML19 alloy. It is established that the presence of Zn in alloys with REMs, when the Zn/REM weight ratio is of about 1.7, makes it possible to attain the precipitation of highly dispersed $MgZn_2$ and $Mg_{12}Nd$ particles, which increases the alloy strength [20]. However, even a small amount of Zn in Mg–Zr–REM alloys increases the creep resistance [11, 21]. In addition, the presence of zinc also somewhat increases the alloy strength [11] and hardness after aging [6]; therefore, its use in the alloy composition makes it possible to decrease the content of high-cost yttrium.

Thus, the ML19 alloy is in many cases a low-cost alternative to materials of the WE43 and WE54 type and, in connection with this, is very interesting for industrial use. However, it is almost unknown outside Russia and has no standardized analogs; therefore, there is not a lot of data about it. The goal of this study is to describe the solidification of this alloy, its structure, and its properties in as cast and heat treated condition.

EXPERIMENTAL

We used pure materials as the charge, notably, magnesium (99.9% Mg) (SMZ, Solikamsk); zinc (99.98% Zn) and the Mg–15% Zr master alloy (SOMZ, Solikamsk); commercial ML10 magnesium alloy containing 2.36% Nd, 0.27% Zn, and 0.51% Zr (SOMZ); and master alloys Mg–20% Nd and Mg–20% Y (OOO PK Metagran, Moscow). The alloy weight for each melting was 300 g. Melting was performed under a flux based on carnallite ($KCl \cdot MgCl_2$) in a high-frequency induction furnace in steel crucibles. Other charge components were introduced after melting the ML10 magnesium alloy in order to acquire the required chemical composition. The Mg–Zr master alloy was added last, after which the melt was held for 15 min at 760–780°C. The melt was poured into a metallic mold at $t = 760$°C in order to fabricate ingots 35 mm in diameter and 140 mm in height, from which the samples for hardness determination and metallographic sections were prepared.

The alloy microstructure and content of elements in phases were investigated using a Tescan Vega SBH3 scanning electron microscope (SEM) with an energy-dispersive microanalysis system (Oxford).

The chemical composition of prepared alloys was determined by energy dispersive X-ray spectroscopy (EDS) on an area of 1 × 1 mm and is presented in Table 2.

The Brinell hardness was evaluated using a Nemesis 9001 universal hardness meter (Innovatest). The following testing parameters were used: a ball 2.5 mm in diameter, a load of 62.5 kgf (≈61.3 kN), and a holding time under a load of 30 s.

Table 2. Composition of prepared alloys

Alloy	Content of elements, wt %				
	Mg	Zn	Y	Zr	Nd
Y1Nd2	Bal.	0.1	1.2	0.6	1.9
Y2Nd3	Bal.	0.7	2.0	0.7	2.6
Y2Nd2*	Bal.	0.5	1.8	0.5	2.0

* Alloys for mechanical tests were prepared from the Y2Nd2 alloy.

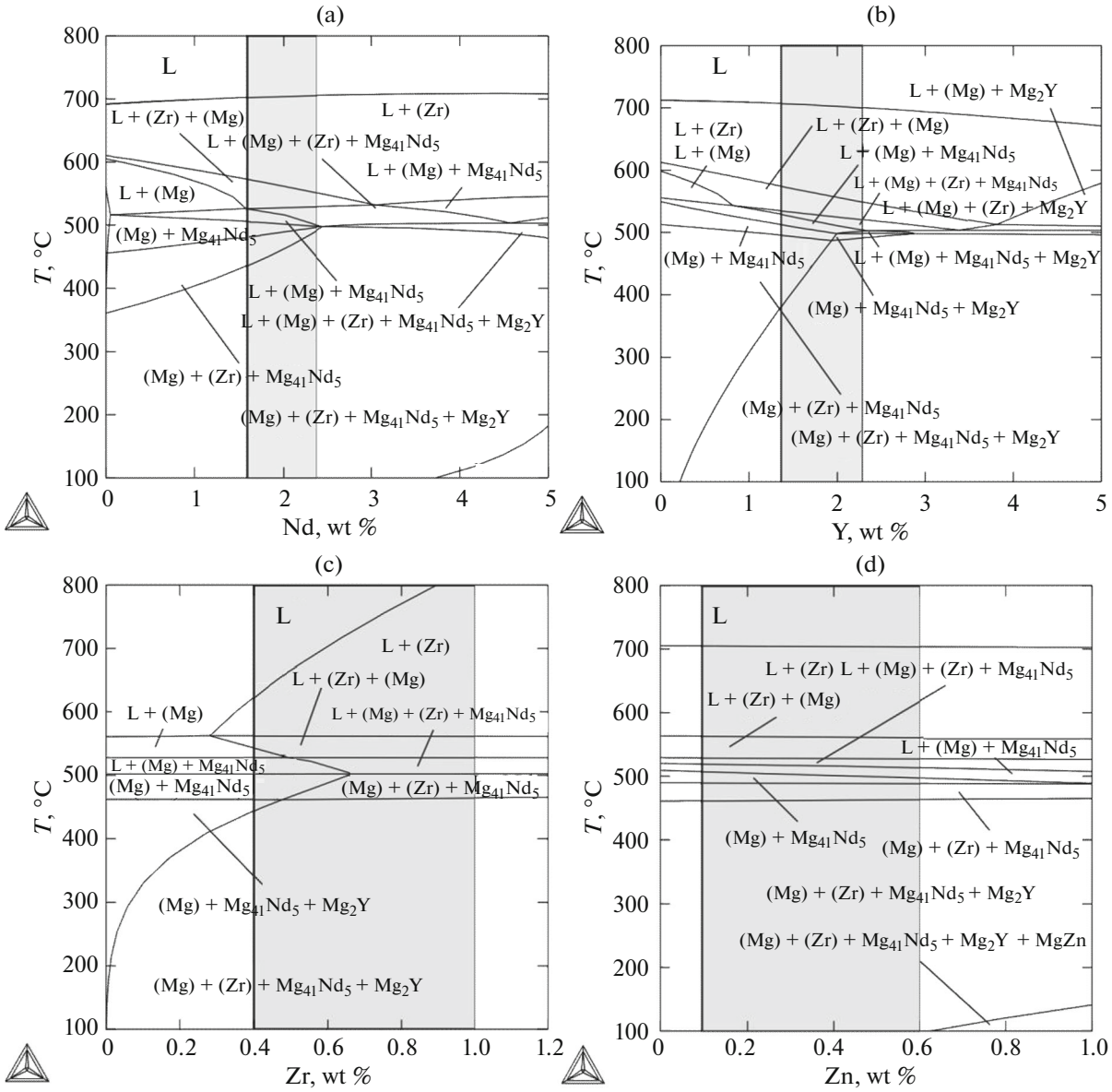

Fig. 1. Polythermal sections of the Mg–Zn–Zr–Nd–Y phase diagram. (a) Mg–0.35% Zn–0.6% Zr–1.8% Y–(0–5)% Nd, (b) Mg–0.35% Zn–0.6% Zr–2% Nd–(0–5)% Y; (c) Mg–0.35% Zn–2% Nd–1.8% Y–(0–1.2)% Zr, and (d) Mg–0.6% Zr–2% Nd–1.8% Y–(0–1)% Zn.

The samples were investigated in as cast and heat treated conditions. To determine the mechanical properties of the alloy, another melting was performed according to the above-described technology. It was performed in a resistance furnace using a steel crucible with a large volume. The ingots for milling the samples according to *GOST 1583–93* of 20 mm in diameter were poured into a steel mold. Mechanical properties were determined using cylindrical samples 5 mm in diameter (type III according to *GOST 1497–84*) milled from cast ingots after their heat treatment. Tensile tests were performed using an Instron 5569 universal testing machine.

Polythermal sections of phase diagrams, the phase composition, and the solidification of alloys according to the Scheil–Gulliver model were calculated using the Thermo-Calc 2016a program [22] and TTMG3 thermodynamic database (Magnesium Alloys Database, version 3) [23].

RESULTS AND DISCUSSION

Equilibrium Solidification of the Alloy

Figure 1 shows polythermal sections of the Mg–Zn–Zr–Nd–Y phase diagram in the concentration field of the ML19 alloy. The influence of the variation

in the concentration of each of the alloying elements (AE) in limits determined by the standard (gray regions) on temperatures of phase transformations at the average (relative to the grade one) content of other alloying elements is shown.

Equilibrium solidification starts upon attaining the equilibrium liquidus temperature by the alloy (t ~ 700°C at a content of 0.6% Zr) from the solidification of primary crystals of almost pure zirconium (Fig. 1a) with an insignificant impurity of other AEs (Zr) from liquid. Then the crystals of the magnesium solid solution (Mg) start to appear upon lowering the temperature to 573–552°C (depending on the neodymium content) from liquid according to the peritectic reaction

$$L + (Zr) \rightarrow (Mg).$$

Upon attaining t ~ 530°C, the peritectic reaction proceeds

$$L + (Zr) \rightarrow (Mg) + Mg_{41}Nd_5,$$

which resulted in the formation of the $Mg_{41}Nd_5$ intermetallic phase along with (Mg). During this process, zirconium-based crystals (Zr) dissolve completely in range t = 530–500°C. It is noteworthy that an increase in the Nd concentration in the alloy (Fig. 1a) extends the temperature range of the peritectic reaction. Alloy solidification is finished by the eutectic reaction

$$L \rightarrow (Mg) + Mg_{41}Nd_5.$$

Herewith, the equilibrium solidus temperature somewhat decreases from 507 to 500°C with an increase in the neodymium concentration.

An increase in the yttrium concentration in the alloy in the limits of its grade composition (Table 1) exert no substantial effect on the alloy liquidus temperature (Fig. 1b). The alloy enters the formation region of the Mg_2Y compound immediately from liquid at t ~ 520°C at an average content of other AE and an increase of yttrium content to 2%. This phase is formed only in a solid state at a lower yttrium concentration.

The zirconium content very strongly affects the alloy liquidus temperature (Fig. 1c). It exceeds 800°C at its maximally admissible amount in the ML19 alloy (1% Zr). Such a temperature is usually not applied when melting magnesium alloys because of the danger of their contamination with undesirable impurities and increased process metal losses. Therefore, the zirconium content in the alloy possible in technology is limited by 0.8%. The zirconium concentration does not affect the solidus temperature.

The presence of zinc in the ML19 alloy in the amount determined by the standard almost does not affect the liquidus temperature and very insignificantly lowers the alloy solidus temperature (Fig. 1d). Herewith, zinc does not form new equilibrium phases.

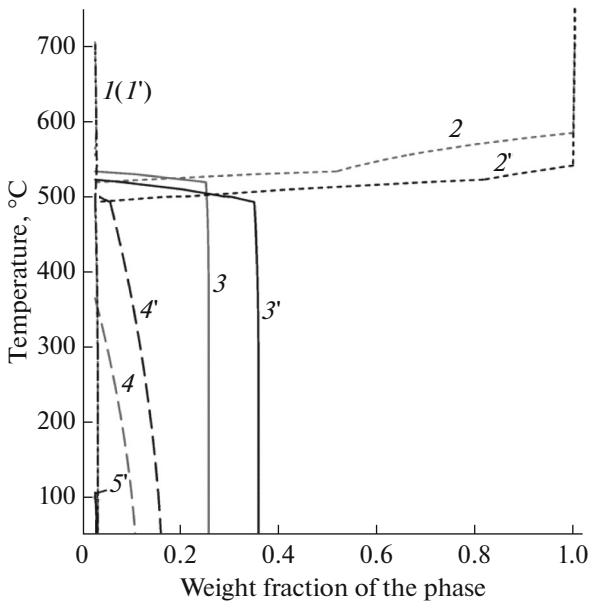

Fig. 2. Variation in the weight fraction of phases in alloys Mg–0.1% Zn–0.6% Zr–1.6% Nd–1.4% Y (*1*–*4*) and Mg–0.6% Zn–0.6% Zr–2.3% Nd–2.2% Y (*1'*–*5'*) depending on temperature. Curves *1*, *1'* correspond to (Zr); curves *2*, *2'* correspond to *L*; curves *3*, *3'* correspond to $Mg_{41}Nd_5$; curves *4*, *4'* correspond to Mg_2Y; and curve *5'* corresponds to MgZn.

The variation in the weight fraction of phases in the ML19 alloy calculated in the Thermo-Calc program depending on temperature is presented in Fig. 2. It is seen that, because of the variable yttrium solubility in the (Mg) solid solution, the amount of the Mg_2Y phase decreases with an increase in temperature. The weight fraction of other phase components varies insignificantly with the variation in temperature.

Nonequilibrium Alloy Solidification

Nonequilibrium solidification was considered using calculations according to the Scheil–Gulliver model in the Thermo-Calc program [24, 25]. Results of the calculation can disagree with the actual process because of the absence of diffusion in the solid phase according to this model, but they will give the notion of nonequilibrium phases and the nonequilibrium solidus temperature, which is important to determine the possible heat treatment temperature.

Figure 3 shows the temperature dependence of the fraction of the solid phase for the equilibrium and nonequilibrium solidification of the ML19 alloy containing alloying elements Nd, Y, and Zn by the lower (Mg–0.6% Zr–0.1% Zn–1.5% Nd–1.4% Y) and upper (Mg–0.6% Zr–0.6% Zn–2.3% Nd–2.2% Y) limits determined according to *GOST*. The Zr content in both alloys is identical, being 0.6%, which is its average value according to the standard.

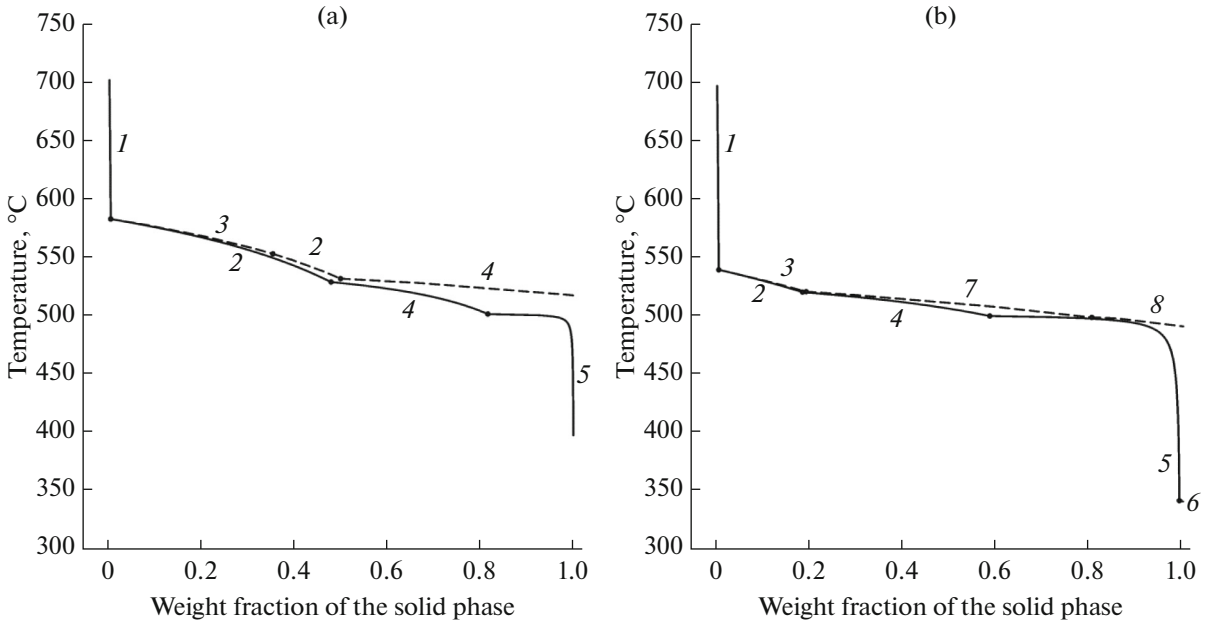

Fig. 3. Solidification pathway of alloys (a) Mg–0.6% Zr–0.1% Zn–1.5% Nd–1.4% Y and (b) Mg–0.6% Zr–0.6% Zn–2.3% Nd–2.2% Y. Phase regions during the equilibrium (the dashed line) and nonequilibrium (the solid line) solidification: (*1*) L + (Zr), (*2*) L + (Mg), (*3*) L + (Mg) + (Zr), (*4*) L + (Mg) + $Mg_{41}Nd_5$, (*5*) L + (Mg) + $Mg_{41}Nd_5$ + Mg_2Y, (*6*) L + (Mg) + $Mg_{41}Nd_5$ + Mg_2Zn_3, (*7*) L + (Zr) + (Mg) + $Mg_{41}Nd_5$, and (*8*) L + (Zr) + (Mg) + $Mg_{41}Nd_5$ + Mg_2Y.

Both equilibrium and nonequilibrium solidification in both alloys (Fig. 3) start from the solidification the primary crystals of zirconium (Zr). Then the magnesium solid solution (Mg) is solidified from the liquid. The $Mg_{41}Nd_5$ intermetallic phase starts to solidify from the liquid along with (Mg) upon attaining temperatures of 531 and 523°C for alloys with low (Fig. 3a) and high (Fig. 3b) contents of alloying components, respectively. Then crystals of the Mg_2Y phase start to form from liquid at t ~500°C. This stage finishes the solidification for the alloy with small AE additions (Fig. 3a). The solidification of the alloy with the AE content according to the lower limit is finished at t ~ 400°C, and, for the alloy with AE according to the upper limit (Fig. 3b), at 343°C, with the formation of a small amount of the Mg_2Zn_3 nonequilibrium eutectic phase.

Thus, the solidus temperature for the completely nonequilibrium solidification is 120–150°C lower (at the minimal and maximal AE contents, respectively) than in equilibrium conditions. This fact should be taken into account when performing the heat treatment of alloys in as cast condition in order to avoid the melting of the nonequilibrium eutectic.

Alloy Microstructure

The microstructure of the samples of alloys Y1Nd2 and Y2Nd3 (Table 2) in as cast condition is presented in Fig. 4. It is seen that it consists of dendrites of the magnesium solid solution (Mg) and bright phases, which are arranged along the boundaries and in the center of dendritic cells.

Zirconium (Zr) particles are met in the center and along the boundaries of dendritic cells; they are most often contain yttrium. In addition, zirconium-containing phases are usually contaminated with iron, silicon, manganese, and more rarely with other impurities.

The results of energy dispersive X-ray spectroscopy show that the bright phase arranged along the boundaries of dendritic cells in the Y1Nd2 alloy has an average composition, at %, of Mg–4.9% Nd–0.9% Zn–1.0% Y; in the Y2Nd3 alloy it is Mg–4.0% Nd–2.4% Zn–1.7% Y. This means that the bright phase along the boundaries of dendritic cells is a eutectic mixture consisting of several intermetallic compounds containing Mg, Nd, Y, and Zn. The presence of Mg_2Y and Mg_2Zn_3 compounds is possible in addition to the $Mg_{41}Nd_5$ phase according to calculations of the nonequilibrium solidification in the Thermo-Calc program. Phases in alloys of the WE43 type are identified in references [26, 27] as $Mg_{24}Y_5$ and $Mg_{14}Nd_2Y$, and their presence is also possible in the ML19 alloy.

The distribution of alloying components over the cross section of the dendritic cell (Mg) is presented in Fig. 5. It is seen that there is an inclusion containing Zr and Y in the dendritic cell center; increased Y and Nd concentrations are observed on its boundary (the bright region to the left); and Zn is present, in addition to Nd and Y, in the eutectic phase to the right.

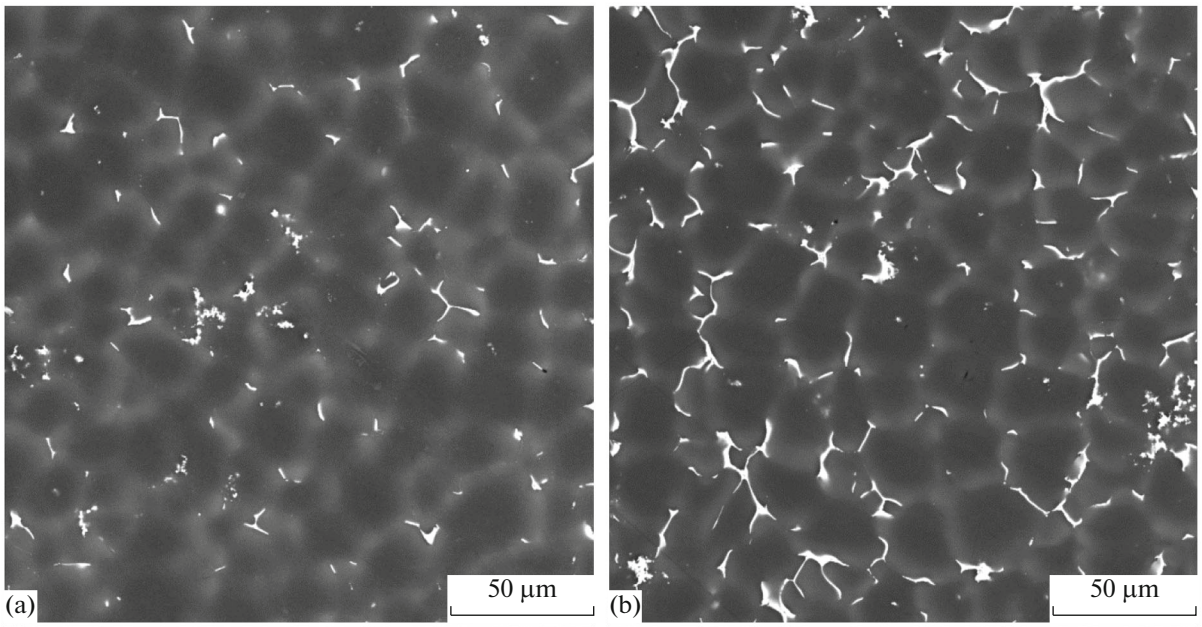

Fig. 4. Microstructure of alloys (a) Y1Nd2 and (b) Y2Nd3 in as cast condition (SEM).

Selection of Heat Treatment Regime

Artificial aging after preliminary quenching at an elevated temperature (Table 3) is traditionally used as the heat treatment (HT) mode for alloys of the Mg–Zn–Zr–REM system. Preliminary quenching with or without subsequent aging is usually performed for the maximal dissolution of alloying components in magnesium solid solution (Mg) in order to attain its maximal strengthening due to the large number of precipitates of the strengthening phase formed during artificial aging. HT according to the T6 mode (Table 3) improves the mechanical properties of the cast alloy mainly due to the decomposition of the supersaturated solid solution of zinc, REM, and zirconium in magnesium formed after high-temperature holding of the casting with subsequent rapid cooling.

Starting from the considered peculiarities of the equilibrium and nonequilibrium solidification of the ML19 alloy, we investigated several HT regimes in order to evaluate their influence on the alloy properties and structure (Table 3). We proposed an alternative alloy HT mode directed to the gradual dissolution of nonequilibrium phases, which includes two-stage alloy heating for quenching and aging (Table 3, HT2 regime). Regimes HT1, HT3, and HT4 are recommended in references for HT of ML19 and WE43 alloys. The use of HT regimes recommended for WE43 is also possible for the ML19 alloy because their phase compositions and solidus temperatures are similar.

Microstructures of alloys after heat treatment according to HT1–HT4 regimes (Table 3) are shown in Fig. 6. It is seen that the structures of all the samples

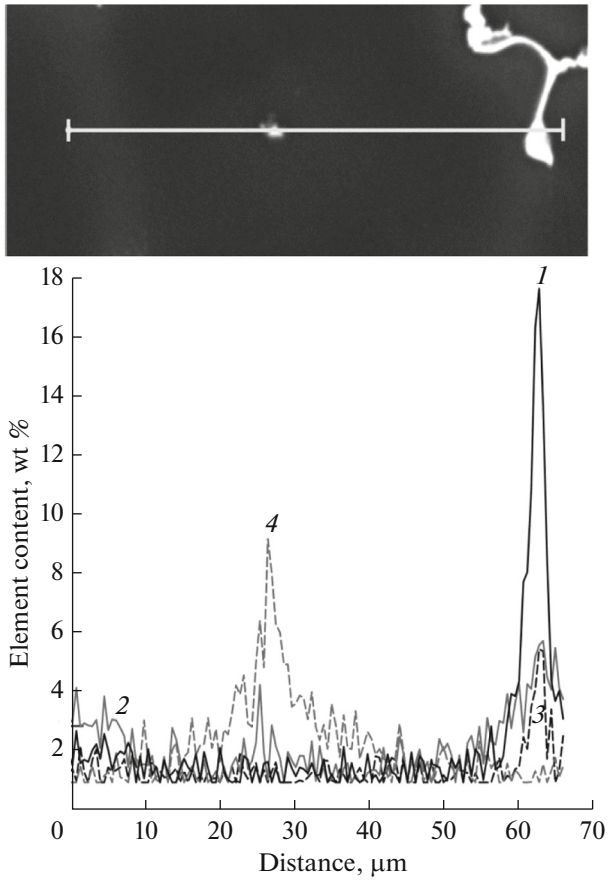

Fig. 5. Distribution of alloying components over the cross section of the dendritic cell of the magnesium solid solution (Mg). (*1*) Nd, (*2*), Y, (*3*) Zn, and (*4*) Zr.

Table 3. Experimental heat treatment regimes for the ML19 alloy

HT	Recommended for alloy	Heating mode before quenching	Environment for quenching	Aging mode	Environment for cooling	Source
HT1	ML19	430°C, 2 h + 535°C, 4 h	Water	205°C, 12 h	Air	[3]
HT2	ML19	400°C, 2 h + 500°C, 8 h	Water	200°C, 16 h	Air	This publication
HT3	WE 43	525°C, 8 h	Water	250°C, 16 h	Air	[13]
HT4	ML19	535°C, 8 h	Water	205°C, 16 h	Air	*OST* (Branch Standard) *190121–90*

after HT are similar. This structure consists of grains of the magnesium solid solution (Mg), inside which the particles of the zirconium-enriched phase (Zr) are present, and regions of needle-shaped phases isolated from the solid solution are formed around it as an initiating center. The sample heat treated according to the HT2 regime is the exclusion (Fig. 6b). Incompletely dissolved regions of intermetallic compounds

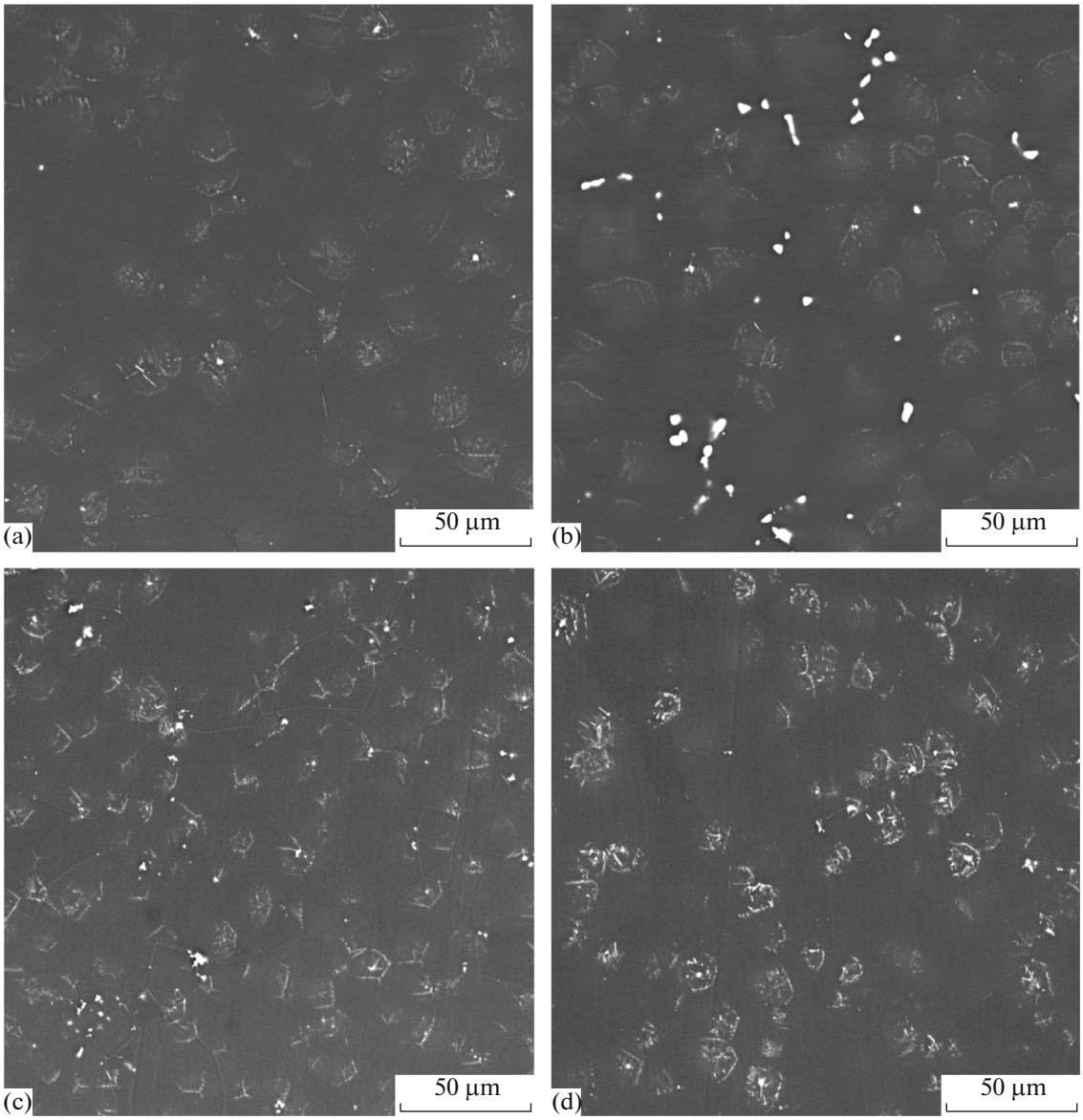

Fig. 6. Microstructure of the Y2Nd2 alloy (see the composition in Table 2) in the heat treated condition (Table 3). (a) HT1, (b) HT2, (c) HT3, and (d) HT4.

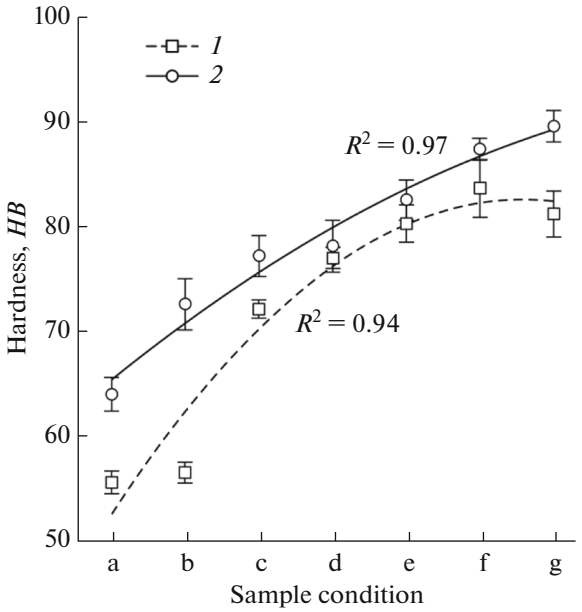

Fig. 7. Variation in hardness of alloys (*1*) Y1Nd2 and (*2*) Y2Nd3 during heat treatment. (a) As cast condition; (b) holding 400°C, 2 h + 500°C, 8 h, with subsequent quenching in water; and (c, d, e, f, g) aging for 4, 8, 12, 16, and 20 h, respectively.

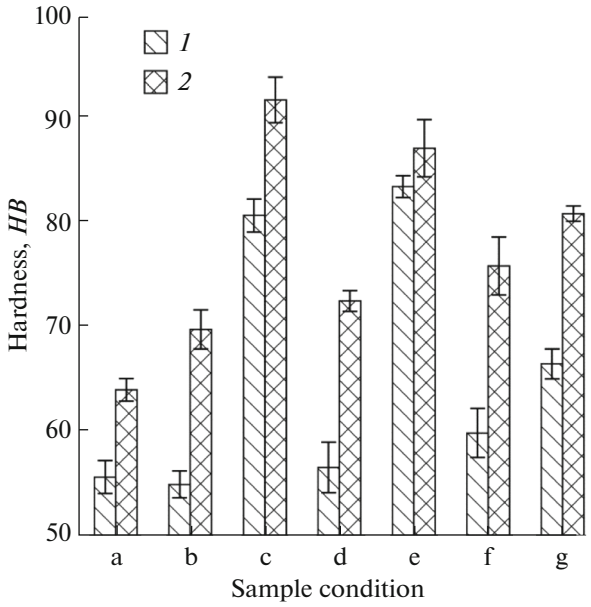

Fig. 8. Variation in hardness of alloys (*1*) Y1Nd2 and (*2*) Y2Nd3 during heat treatment. (a) As cast condition; (b, d, f) quenching according to HT1, HT2, and HT3 regimes; and (c, e, g) aging according HT1, HT2, and HT3 regimes (Table 3).

along grain boundaries are observed in it, which is a consequence of the lower (500°C against 525–535°C) temperature of the alloy HT for quenching. In addition, it is distinguishable that the grain boundaries in alloys aged at t = 200–205°C (Figs. 6a, 6b, 6d) are pronounced less clearly than in the sample aged at 250°C (Fig. 6c).

Our experimental results show that the plot of varying the weight fraction of phases in alloys Mg–0.1% Zn–0.6% Zr–1.6% Nd–1.4% Y (curves *1–4* in Fig. 2) and Mg–0.6% Zn–0.6% Zr–2.3% Nd–2.2% Y (curves *1'–5'* in Fig. 2), depending on temperature and the data on the temperature of phase transformations (Fig. 1), are not quite correct. Melting of grains should be observed by the results of calculations at a HT temperature of 535°C for the ML19 alloy, which is not found experimentally.

Mechanical Properties of Alloys

The optimal aging time was determined for Y1Nd2 and Y2Nd3 samples from the ML19 alloy subjected to isothermal holding with subsequent quenching in water. Holding was performed at 400°C for 2 h (to dissolve nonequilibrium phases) and at 500°C for 8 h. Quenched alloys Y1Nd2 and Y2Nd3 were subjected to aging at 200°C with the measurement of their hardness for equal time intervals. The results of determining *HB* are presented in Fig. 7. It is seen that alloys reach the maximal hardness with an aging duration of 16–20 h; precisely this aging time was used for alloy HT according to HT2 regime (Table 3).

The hardness of the samples heat treated according to HT1, HT2, and HT3 modes is presented in Fig. 8. No testing was performed for the alloy after HT4 because this regime is similar to HT1 and, most likely, the samples will have similar *HB* after the HT. It is seen that the maximal hardness of the Y1Nd2 alloy can be observed when using the HT2 mode, while the minimal one can be observed after HT3. The hardness of the Y2Nd3 alloy with an increased content of alloying components is largest after HT according to the HT1 regime. We note that the hardness of the Y2Nd3 alloy after HT according to all modes is higher than that of the Y1Nd2 alloy. Low *HB* of the samples heat treated according to the HT3 mode evidences a not very high aging temperature. These data coincide with the results of other authors [18, 19] and are explained by the transformation of metastable phases precipitating during sample aging into stable ones.

Tensile tests of the samples of the Y2Nd2 alloy after HT according to various regimes (Fig. 9) showed that the maximal strength was attained when using the HT2 regime (Table 3). The application of the HT3 mode recommended for WE43 and WE54 alloys for the ML19 alloy leads to a decrease in the alloy strength and an increase in its elongation at room temperature. Heat treatment according to HT1 and HT4 regimes showed an approximately identical result with a somewhat larger elongation attained when using the HT1 mode.

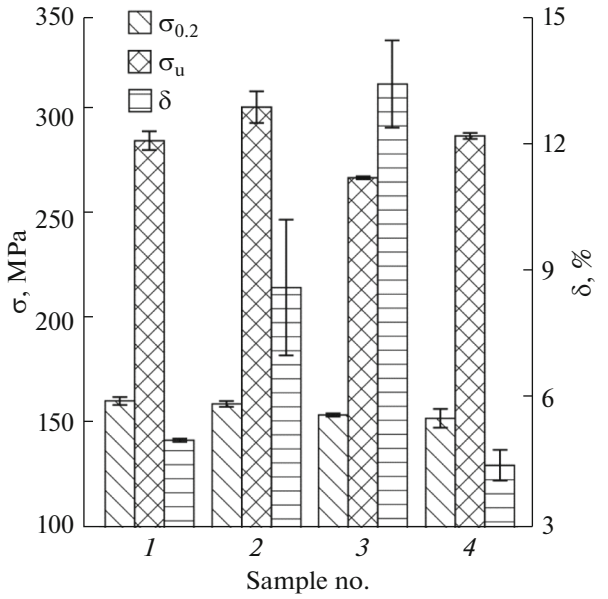

Fig. 9. Results of mechanical tensile testing of the Y2Nd2 alloy heat treated according to various regimes (Table 3). (*1*) HT1, (*2*) HT2, (*3*) HT3, and (*4*) HT4.

Thus, an increase in the alloy aging temperature to 250°C decreases its room-temperature strength but increases elongation, which confirms conclusions done for the WE43 alloy in [18, 19]. High strength and plasticity characteristics can be attained even when no complete dissolution of the intermetallic phase occurs due to a decrease in the solutionizing temperature to 500°C.

CONCLUSIONS

(i) An increase in the zirconium content in the ML19 alloy more than 0.8–0.9% requires an increase in the melting temperature above 800°C, which is undesirable from the process viewpoint when melting the alloy in a steel crucible and, consequently, is unreasonable in industrial conditions.

(ii) The nonequilibrium solidus temperature of the ML19 alloy is lower by approximately 120–150°C (at minimal and maximal contents of alloying elements, respectively) than under equilibrium conditions. This fact should be taken into account during the alloy HT in order to avoid the melting of nonequilibrium eutectic. It was established that alloy holding at 400°C for 2 h completely excludes the danger of nonequilibrium eutectic melting.

(iii) The best room-temperature mechanical properties of the ML19 alloy were attained when using the HT included the two-stage heating (400°C, 2 h + 500°C, 8 h) and quenching in water with subsequent aging at 200°C for 16 h. Herewith, a ultimate strength of 306 ± 8 MPa, elongation of 8.7 ± 1.6%, and yield strength of 161 ± 1 MPa were attained. However, the application of this mode can lead to the formation of residual intermetallic phases after the HT.

(iv) The use of an increased aging temperature (250°C) for the ML19 alloy leads to a decrease in alloy ultimate strength to 272 ± 1 MPa with an increase in the elongation to 13 ± 1%.

ACKNOWLEDGMENTS

This article was prepared by materials of a study performed in the scope of Statement of the Government of the Russian Federation no. 218 dated April 9, 2010, state contract no. 03.G25.31.0274.

REFERENCES

1. Friedrich, H.E. and Mordike, B.L., *Magnesium Technology: Metallurgy, Design Data, Applications*, New York: Springer, 2006.
2. Mordike, B.L. and Ebert, T., Magnesium: properties-applications-potential, *Mater. Sci. Eng. A*, 2001, vol. 302, no. 1, pp. 37–45.
3. Rokhlin, L.L., *Magnesium Alloys Containing Rare Earth Metals: Structure and Properties*, London: Taylor & Francis, 2003.
4. Antion, C., Donnadieu, P., Deschamps, A., Tassin, C., and Pisch A., Hardening precipitation in a Mg–4Y–3RE alloy, *Acta Mater.*, 2003, vol. 51, no. 18, pp. 5335–5348.
5. Polmear, I.J., Magnesium alloys and applications, *Mater. Sci. Technol.*, 1994, vol. 10, no. 1, pp. 1–16.
6. Penghuai, F., Liming, P., Haiyan, J., Jianwei, C., and Chunquan, Z., Effects of heat treatments on the microstructures and mechanical properties of Mg–3Nd–0.2Zn–0.4Zr (wt %) alloy, *Mater. Sci. Eng. A*, 2008, vol. 486, nos. 1–2, pp. 183–192.
7. Nie, J.F. and Muddle, B.C., Characterisation of strengthening precipitate phases in a Mg–Y–Nd alloy, *Acta Mater.*, 2000, vol. 48, pp. 1691–1703.
8. Zhao, H.D., Qin, G.W., Ren, Y.P., Pei, W.L., Chen, D., and Guo, Y., The maximum solubility of Y in α-Mg and composition ranges of $Mg_{24}Y_{5-x}$ and Mg_2Y_{1-x} intermetallic phases in Mg–Y binary system, *J. Alloys Compnd.*, 2001, vol. 509, no. 3, pp. 627–631.
9. Chia, T.L., Easton, M.A., Zhu, S.M., Gibson, M.A., Birbilis, N., and Nie, J.F., The effect of alloy composition on the microstructure and tensile properties of binary Mg–rare earth alloys, *Intermetallics*, 2009, vol. 17, no. 7, pp. 481–490.
10. Rokhlin, L.L., Dobatkina, T.V., Tarytina, I.E., Timofeev, V.N., and Balakhchi, E.E., Peculiarities of the phase relations in Mg-rich alloys of the Mg–Nd–Y system, *J. Alloys Compnd.*, 2004, vol. 367, nos. 1–2, pp. 17–19.
11. Mukhina, I.Yu., Duyunova, V.A., Frolov, A.V., and Uridiya, Z.P., Effect of RE alloying on the high-temperature strength of casting magnesium alloys, *Metal. Mashinostr.*, 2014, no. 5, pp. 34–38.
12. Vinotha, D., Raghukandan, K., Pillai, U.T.S., and Pai, B.C., Grain refining mechanisms in magnesium

alloys—An overview, *Trans. Indian Inst. Met.*, 2009, vol. 62, pp. 521–532.

13. Changjiang, S., Qingyou, H., and Qijie, Z., Review of grain refinement methods for as-cast microstructure of magnesium alloy, *China Foundry*, 2009, vol. 6, pp. 93–103.
14. Polmear, I.J., *Light Alloys, Oxford*: Butterworth–Heinemann, 2005, 4th ed.
15. *Heat Treater's Guide: Practices and Procedures for Nonferrous Alloys*, Chandler, H., Ed., Ohio: ASM International, 1996.
16. Nie, J.F. and Muddle, B.C., Precipitation in magnesium alloy WE54 during isothermal ageing at 250°C, *Scr. Mater.*, 1999, vol. 40, no. 10, pp. 1089–1094.
17. Nie, J.F., Effects of precipitate shape and orientation on dispersion strengthening in magnesium alloys, *Scr. Mater.*, 2003, vol. 48, no. 8, pp. 1009–1015.
18. Mengucci, P., Barucca, G., Riontino, G., Lussana, D., Massazza, M., Ferragut, R., and Hassan, Aly E., Structure evolution of a WE43 Mg alloy submitted to different thermal treatments, *Mater. Sci. Eng. A*, 2008, vol. 479, nos. 1–2, pp. 37–44.
19. Kumar, N., Choudhuri, D., Banerjee, R., and Mishra, R.S., Strength and ductility optimization of Mg–Y–Nd–Zr alloy by microstructural design, *Int. J. Plast.*, 2015, vol. 68, pp. 77–97.
20. Feng, H., Liu, H., Cao, H., Yang, Y., Xu, Y., and Guan, J., Effect of precipitates on mechanical and damping properties of Mg–Zn–Y–Nd alloys, *Mater. Sci. Eng. A*, 2015, vol. 639, pp. 1–7.
21. Suzuki, M., Kimura, T., Koike, J., and Maruyama, K., Effects of zinc on creep strength and deformation substructures in Mg–Y alloy, *Mater. Sci. Eng. A*, 2004, vols. 387–389, pp. 706–709.
22. Andersson, J.O., Helander, T., Hoglund, L., Shi, P.F., and Sundman, B., Thermo-Calc and DICTRA, computational tools for materials science, *CALPHAD*, 2002, vol. 26, pp. 273–312.
23. *Thermo-Calc Software TTMG3 Magnesium Alloys Database*, version 3, accessed June 1, 2017.
24. Gulliver, G.H., The quantitative effect of rapid cooling upon the constitution of binary alloys, *J. Inst. Met.*, 1913, vol. 9, pp. 120–157.
25. Scheil, E., Bemerkungen zur Schichtkristallbildung, *Zeitschrift für Metallkunde*, 1942, vol. 34, pp. 70–72.
26. Zhang, H., Fan, J., Zhang, L.WuG., Liu, W., Cui, W., and Feng, S., Effect of heat treatment on microstructure, mechanical properties and fracture behaviors of sand-cast Mg–4Y–3Nd–1Gd–0.2Zn–0.5Zr alloy, *Mater. Sci. Eng. A*, 2016, vol. 677, pp. 411–420.
27. Rzychon, T. and Kielbus, A., Microstructure of WE43 casting magnesium alloys, *J. Achiev. Mater. Manuf. Eng.*, 2007, vol. 21, pp. 31–34.

Translated by N. Korovin